PNAS RESEARCH ARTICLE | PHARMACOLOGY

Flycodes enable simultaneous preclinical analysis for dozens of antibodies in single cassette–dosed mice

Justin D. Walter[a,1,2], Michal Beffinger[b,1], Pascal Egloff[a,1], Iwan Zimmermann[a,c], Lea M. Hürlimann[c], Fabian Ackle[a], Matthias Seifert[d], Sebastian Kobold[d,e,f], Johannes vom Berg[b,3], and Markus A. Seeger[a,3]

Affiliations are included on p. 10.

Edited by James Wells, University of California San Francisco, San Francisco, CA; received December 30, 2024; accepted February 13, 2025

Protein therapeutics such as antibodies require in-depth in vivo characterization during development and consequently account for a large proportion of laboratory animal consumption in the pharmaceutical industry. Currently, antibody candidates are exhaustively tested one-by-one in animal models to determine pharmacokinetic and pharmacodynamic (PK/PD) profiles. The simultaneous analysis of antibody mixtures in single animals, called cassette-dosing, could in principle overcome this bottleneck, but is currently limited to small cassette sizes. Here, we demonstrate how the use of genetically encoded peptide tags (flycodes), designed for maximal detectability in liquid chromatography-mass spectrometry, can allow for the simultaneous characterization of large pools of drug candidates, from single cassette–dosed mice. We demonstrate the simultaneous assessment of PK parameters for a group of >20 marketed/development-stage antibodies. Biodistribution experiments in mice bearing EGFR-expressing tumors correctly identified the two pool members recognizing EGFR, while organ analysis registered liver accumulation of an antibody targeting glucagon receptor, a protein profoundly expressed in that organ. In analogy to an early-phase drug development campaign, we performed biophysical and PK analysis for a cassette of 80 unique bispecific DARPin-sybody molecules. The data shown in this study originate from only 18 cassette-dosed mice, thereby demonstrating how flycode technology efficiently advances preclinical discovery pipelines allowing a direct comparison of drug candidates under identical experimental conditions.

cassette dosing | antibodies | sybodies | flycodes | mass spectrometry

Significance

During discovery and development of protein-based biotherapeutics, extensive preclinical animal testing is required for assessment of drug behavior, efficacy, and safety. Generally, numerous animals are required for testing an individual biotherapeutic drug candidate. We show that the use of genetically encoded peptide barcodes, called flycodes, allows for the simultaneous assessment of 25 clinically relevant antibodies from single cassette–dosed mice. We also used flycodes to efficiently measure biophysical characteristics and pharmacokinetic data for a set of 80 drug-like synthetic biomolecules, effectively mimicking the early development stage of the biotherapeutic development pipeline while using minimal resources. Our results show that flycodes offer a means for obtaining high-quality preclinical data, while potentially reducing the number of required animals by up to 100-fold.

Protein-based biotherapeutics such as monoclonal antibodies have emerged as the fastest-growing category of newly developed drugs, due to their unparalleled target specificity, low toxicity, long-lasting pharmacological effect, and modularity (1, 2). Furthermore, with the expanding repertoire of available formats and scaffolds for antibodies and other engineered binder proteins (3, 4) they will continue to represent one of the most important therapeutic substance classes in the future. However, approximately 85% of protein biotherapeutics that enter phase I clinical trials fail to reach the approval stage (5). Importantly, this metric does not consider the large numbers of discovery-phase candidates that either fail to meet biophysical criteria for entry into preclinical or phase I clinical trials, or are simply never sufficiently characterized due to resource and/or methodology limitations. Conventional antibody selection platforms are capable of routinely generating thousands of potential drug leads, and automation technology has facilitated increased efficiency for in vitro biophysical characterization. However, successful drugs must have favorable pharmacokinetics (PK) and pharmacodynamics (PD). For biotherapeutics, this typically entails slow elimination, precise targeting (e.g. accumulation in the target organ), and limited biodistribution in nontargeted tissues. Unfortunately, despite promising efforts to delineate in vitro and in vivo correlates, PK/PD cannot be reliably predicted from simple biophysical properties (6, 7). Therefore, multiple animals are required to determine PK/PD for each individual biotherapeutic candidate at the preclinical phase. The resulting cost, labor, and ethical burdens necessitate that only relatively few drug candidates are analyzed in early in vivo studies. Therefore, improved methods are needed that allow greater throughput for preclinical PK/PD assessment while reducing animal usage.

One potential solution to the throughput bottleneck in preclinical studies is cassette dosing—the simultaneous administration of a mixture of drug candidates, to a single animal (8). Cassette dosing was originally devised for the rapid in vivo screening of small-molecules, and relies on liquid chromatography–tandem mass spectrometry (LC–MS/MS) for quantitative detection of multiple compounds in a complex plasma mixture. However, problems associated with small-molecule cassette dosing include the high

This article is a PNAS Direct Submission.

[1]J.D.W., M.B., and P.E. contributed equally to this work.

[2]Present address: Molecular Partners AG, Schlieren 8952, Switzerland.

[3]To whom correspondence may be addressed. Email: johannes.vomberg@uzh.ch or m.seeger@imm.uzh.ch.

This article contains supporting information online at https://www.pnas.org/lookup/suppl/doi:10.1073/pnas.2426481122/-/DCSupplemental.

Published March 17, 2025.

incidence of drug–drug interactions, competitive binding with metabolic enzymes, and low solubility, which may result in inaccurate PK assessment. In contrast, the high specificity, alternate clearance mechanisms, and high aqueous solubility of biotherapeutic drug candidates such as antibodies would seem to make them ideal for cassette dosing analysis. Yet, biotherapeutics typically lack sufficient distinguishable chemical signatures (i.e. unique endogenous tryptic peptides) for reliable and specific LC–MS/MS detection, making cassette dosing challenging. So far antibody cassette dosing has been achieved only for small cassette sizes up to four entities, thus not matching the recent progress with regard to the throughput of earlier phases of the drug development (9–11).

To mitigate this bottleneck in the development of biotherapeutics, we present here an approach that enables larger numbers of biotherapeutic proteins to be analyzed in vivo by cassette dosing. Our technology pipeline relies on genetically encoded peptide barcodes called flycodes (12), which are designed for maximal detectability via LC–MS/MS. As depicted in Fig. 1, sets of around 30 to 40 different flycodes are C-terminally fused to antibodies or other biomolecules. Upon purification of the biomolecules from tissues or fluids via the His-tag, the flycode sequence (marked red in Fig. 1*B*) is isolated by consecutive thrombin and trypsin cleavage. The flycode consists of 11 to 15 amino acids (length variation occurs at position $Z_{0\text{-}4}$) and contains a stretch of seven randomized residues (X_7). Neither the randomized stretch (X_7) nor the variable sequence defining the flycode length ($Z_{0\text{-}4}$) contain positively charged residues. Consequently, every flycode has only two positive charges (N-terminus and C-terminal arginine) and falls into the optimal mass range of LC-MS/MS detection (550 to 850 Da).

In the context of this work, flycodes serve as ideal surrogate peptides for identification of all biotherapeutic proteins in complex plasma or tissue samples. Importantly, the use of flycodes as detection surrogates allows the discrimination of near-identical biotherapeutic proteins — a feature that is impossible when relying on unique endogenous tryptic peptides. We demonstrate that flycodes allow the simultaneous PK assessment of >20 marketed or advanced clinical-stage antibodies and enable observation of target-specific tumor accumulation for multiple biotherapeutics from a single cassette–dosing experiment. Additionally, flycodes facilitated PK analysis of 80 highly similar bispecific DARPin-sybody [Designed Ankyrin Repeat Protein (13) – synthetic nanobody (14)] molecules in a single experiment.

Results

Validation of Flycoded Antibodies in Single-Dosed Mice. To validate the use of flycodes for pharmacokinetic analyses, we purified three clinical-stage antibodies, alemtuzumab, rituximab, and cetuximab, each having either around 30 to 40 different flycodes attached (called FC-alemtuzumab, FC-rituximab, and FC-cetuximab) or being devoid of flycodes. In case of cetuximab, the nonflycoded antibody was clinical-grade material not produced by ourselves (*Materials and Methods*). The purified antibodies were injected intravenously (i.v.) into C57BL/6 mice at doses of 1 mg/kg and 10 mg/kg (cetuximab) or 5 mg/kg (alemtuzumab and rituximab). Mouse plasma was collected throughout an 8 d time course, and antibody concentrations in the plasma were determined by ELISA using affinity reagents specific for the

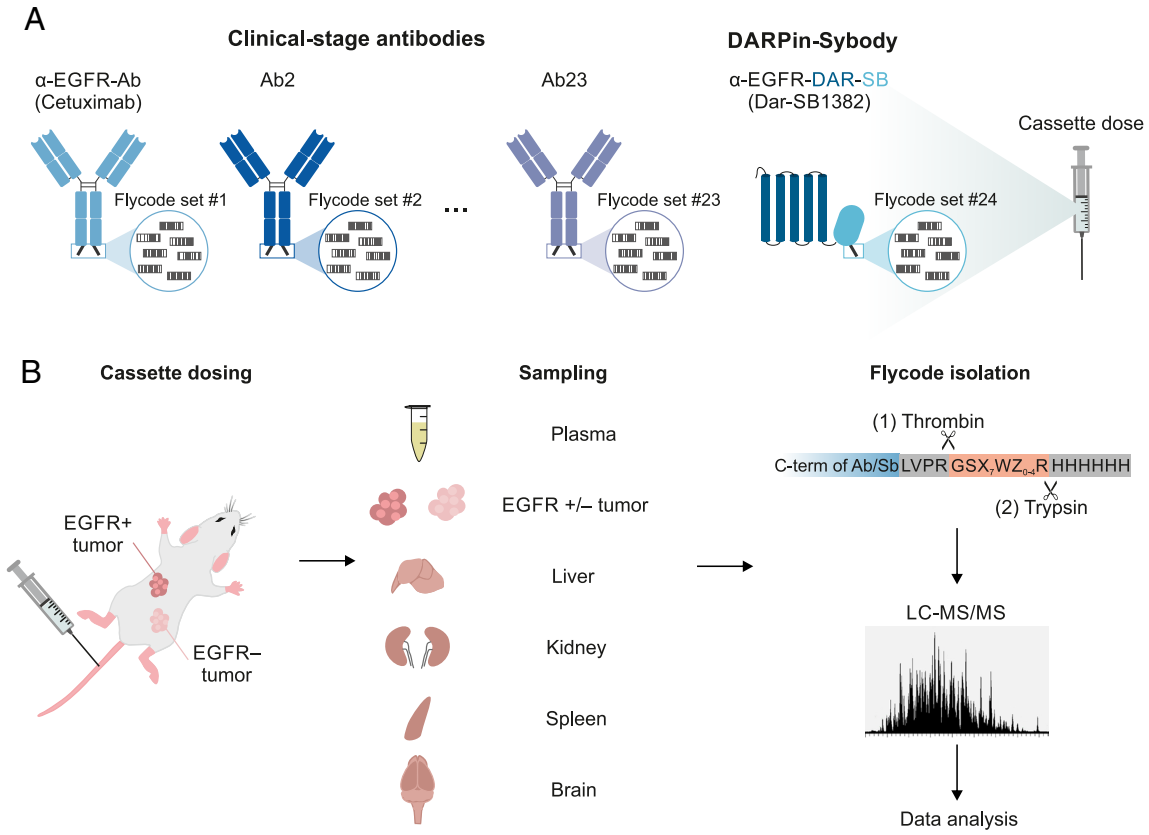

Fig. 1. Overview of flycode-enabled PK/PD analysis of antibody cassette pools. (*A*) Cloning, expression, and purification of a cassette pool of 23 differentially flycoded clinical-stage antibodies (flycode sets #1-23) and a flycoded DARPin-Sybody with the DARPin serving as half-life extension module binding to albumin (flycode set #24). One antibody (cetuximab) and the DARPin-sybody (DAR-SB1382) bind to EGFR. (*B*) The cassette pool is injected into the tail vein of mice implanted with EGFR-expressing LLC tumors on one flank and EFGR-negative LLC tumors on the opposing flank. Plasma, tumors, and organs were sampled. The flycodes are isolated by purifying the cassette pool members via the C-terminal His-tag and by consecutive cleavage by thrombin and trypsin. The flycodes are measured by LC–MS/MS and the resulting data are analyzed.

respective antibodies (*Materials and Methods*). We observed an overall good correlation of the pharmacokinetic curves of flycoded versus nonflycoded antibodies upon data normalization to the first three sampling points after injection (*SI Appendix*, Fig. S1). However, the absolute plasma concentrations of flycoded antibodies were consistently lower. When determining the area under curve (AUC) of the normalized pharmacodynamic curves for the individual mice over the time course of the experiment, flycoded antibodies exhibited somewhat faster clearance than those devoid of flycodes (*SI Appendix*, Fig. S2). In case of cetuximab, the difference may be explained by different cell lines and purification protocols used to produce the flycoded versus the nonflycoded antibody. By contrast, alemtuzumab and rituximab were produced and purified as flycoded and nonflycoded antibodies under identical conditions (*Materials and Methods*). Their mean AUCs for the flycoded versus the nonflycoded versions were reduced by 7 and 25 %, respectively. An unpaired *t* test analysis for the AUC values determined for the individual mice revealed that the differences between flycoded and nonflycoded alemtuzumab and rituximab were nonsignificant ($P > 0.05$), and thus minor. In summary, our ELISA demonstrated that the pharmacokinetic behavior of flycoded antibodies is comparable to those devoid of flycodes.

Next, we assessed the correlation of plasma levels determined by an antibody-specific ELISA or via the flycodes using LC–MS/MS. First, we performed quality-control experiments to verify the suitability of flycodes for antibody quantitation; LC–MS/MS revealed a linear relationship between summed flycode intensities and antibody concentration, as previously reported for flycoded nanobodies (12), allowing for the determination of absolute antibody concentrations via inclusion of internal standards (*SI Appendix*, Fig. S3). We also demonstrated that flycode-based detection allowed for considerably greater accuracy and reliability relative to the use of endogenous tryptic peptides (*SI Appendix*, Fig. S4). Using internal standards, we performed LC–MS/MS to quantify FC-alemtuzumab, FC-rituximab, and FC-cetuximab serum concentrations and plotted the values side-by-side with those obtained from ELISA quantitation, showing generally high correlation between the two detection methods and comparable AUC values (*SI Appendix*, Figs. S1 and S2).

Flycodes Enable Simultaneous Pharmacokinetic analysis of a Pool of Clinical-Stage Antibodies in Cassette-Dosed Mice. We reasoned that relative pharmacokinetic comparisons of cassette pools measured simultaneously by LC–MS/MS will give rise to high-quality datasets that are very difficult to generate using single-dosed mice. Therefore, we selected 23 clinical-phase antibodies, encompassing a variety of targets, disease indications, and immunoglobulin subclasses (Dataset S1). This collection included biosimilar versions of highly successful marketed antibody drugs (e.g. adalimumab, nivolumab, rituximab) as well as development-stage drug candidates (e.g. donanemab, nimacimab, volagidemab). All chosen antibodies were either fully human or humanized mouse IgGs, except for the inclusion of a well-characterized mouse/rat chimeric antibody (m8D3) (15). Each IgG heavy chain gene was differentially ligated to a unique set of 30 to 40 flycodes, and all flycoded antibodies were separately expressed and secreted from mammalian cells, followed by combining of supernatants for one-pot bulk purification (Fig. 1). Notably, the flycoded antibody pool contained a pair of IgGs (denosumab and nivolumab) for which two different heavy-chain variants were produced and separately flycoded: 1) wild-type (unaltered, WT); and 2) H310A/H435Q. The H310A/H435Q variants were included as pharmacokinetic validation controls, since these mutations were reported to reduce elimination half-life approximately 5-fold due to weaker interactions with the neonatal Fc receptor (FcRn) (16).

For pharmacokinetic analysis, the pool of flycoded antibodies was injected intravenously (i.v.) into C57BL/6 mice at a total combined antibody dose of 60 mg/kg (cassette dose A), and an additional cohort of mice received a fourfold diluted pool dose of 15 mg/kg total IgG (cassette dose B) (Fig. 1). Since the antibody pool was purified in bulk, actual doses of the individual antibodies were determined by LC–MS/MS quantification of extracted flycodes from the purified cassette pool and ranged from 0.1 to 6.4 mg/kg for the high-dose cassette A and 0.03 to 1.6 mg/kg for the lower dose cassette B (Dataset S2). All antibodies were readily detected and quantifiable in the input mouse-injection samples, except for cetuximab; this was due to the substantially lower relative expression yields of cetuximab, which we consistently observed (*SI Appendix*, Fig. S5).

Mouse plasma was sampled throughout an 8 d time course and extracted flycodes were quantified using LC–MS/MS, allowing extrapolation of individual antibody concentrations in plasma with high precision when comparing data from different individual mice (*SI Appendix*, Fig. S6). As a further validation, the pharmacokinetic curves determined for alemtuzumab and rituximab in cassette-dosed mice were comparable to those measured in single-dosed mice (*SI Appendix*, Fig. S1). Fig. 2*A* shows plasma concentration-time plots for five representative antibodies from mice of the high-dose (cassette A) cohort, and all plots are shown in *SI Appendix*, Fig. S7. Estimated pharmacokinetic parameters (AUC, clearance, half-life, mean residence time, and volume of distribution) were determined using the PKsolver tool (17) and are presented in Dataset S2. Nearly all of the clinical-stage antibodies displayed characteristic slow elimination behavior that is consistent with the well-known pharmacokinetic properties of IgGs (18). Interestingly, all antibodies showed a slightly delayed T_{max} (time to maximum concentration), with peak serum concentrations occurring at 3 h (0.125 d) postinjection (*SI Appendix*, Fig. S8). While delayed T_{max} is an unexpected phenomenon for intravenous dosing, it has nonetheless recently emerged as a surprisingly frequent PK characteristic of clinical-grade monoclonal antibodies that is also routinely observed in human clinical trial data (19, 20). Several antibodies displayed essentially linear PK between both doses, as illustrated by rituximab (Fig. 2*B*). Conversely, other antibodies showed apparent nonlinear PK, as for volagidemab (Fig. 2*C*), which is indicative of either anti-drug antibodies or target-mediated drug disposition (TMDD), the latter being more likely in this case (21). Interestingly, the murine antibody m8D3 displayed rapid elimination in both cassette doses (Fig. 2*A*). Since m8D3 targets the mouse transferrin receptor (mTfR), this behavior is likely due to efficient TMDD, as previously observed (15). Plozalizumab was quickly eliminated in both cassette dose cohorts (*SI Appendix*, Fig. S7). The rapidity of elimination suggests a pronounced TMDD effect, although the mouse homolog of the human target of plozalizumab (CCR2) shares only 77% sequence identity (Dataset S1) so the cause of this behavior is unclear. Notably, while the WT forms of denosumab and nivolumab show slow elimination behavior, the H310A/H435Q variants of these antibodies displayed markedly accelerated clearance (Fig. 2*D*), consistent with the expected effects of these dual Fc domain mutations (16) and thereby offering further methodological validation. Finally, the utility of flycode-based cassette dosing for direct comparison of several antibodies is illustrated in Fig. 2*E*, which shows the computed clearance values for all antibodies in cassette dose A, ordered from slowest elimination (nivolumab) to fastest (m8D3). Importantly, clearance values show a high correlation between both cassette doses ($R^2 = 0.73$)

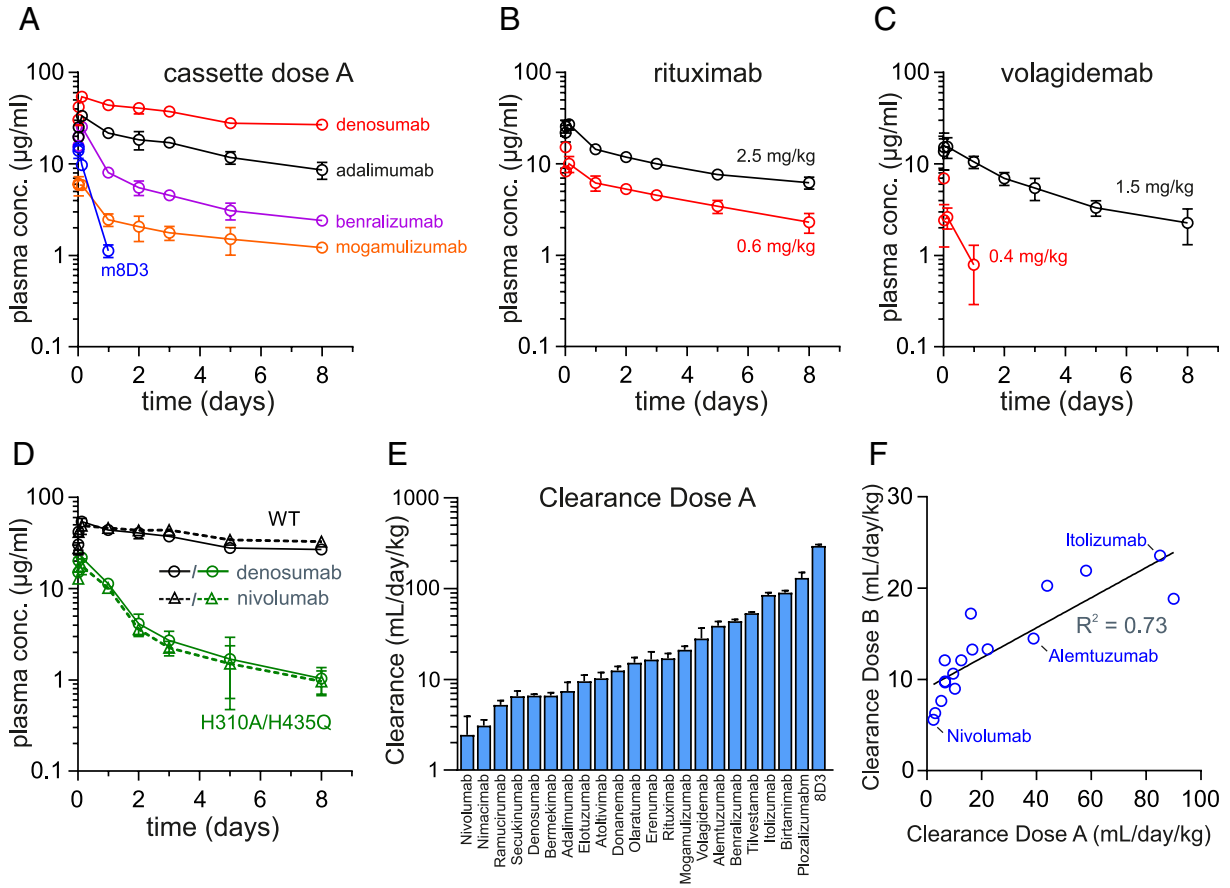

Fig. 2. Flycode-enabled pharmacokinetic analysis of >20 antibodies in cassette-dosed mice. (*A*–*C*) Plasma levels of flycoded antibodies from cassette-dosed mice detected by LC–MS/MS. Sampling time points: 0.01, 0.02, 0.13, 1, 2, 3, 5, and 8 d. (*A*) Plasma concentration vs. time curves for antibodies from cassette dose A (60 mg/kg) detected by LC–MS/MS. Five representative antibody PK curves are highlighted in the indicated colors. See *SI Appendix*, Fig. S7 for all PK curves from both cassette doses. (*B*) Rituximab PK behavior from both cassette dose cohorts, showing linear PK. (*C*) Volagidemab PK behavior from both cassette dose cohorts, showing nonlinear PK. (*D*) Two antibodies engineered to have reduced half-lives could be distinguished from their WT counterparts within a single cassette (dose A). Solid lines and circles, denosumab; dotted lines and triangles, nivolumab. Black, WT sequences; green, H310A+H435Q mutations in antibody Fc domains. (*E*) Clearance values for all antibodies from cassette dose A. (*F*) Comparison of clearance values determined for each antibody in cassette dose A (60 mg/kg) versus cassette dose B (15 mg/kg). Fitted linear regression curve and coefficient of correlation are shown. Data points are the average of three biological replicates, isolated from three different mice. Error bars represent the SD.

(Fig. 2*F*). Overall, these experiments illustrated that flycodes allow for reliable and efficient determination of PK parameters, enabling dramatic throughput increases over traditional methods.

Flycode-Based Tumor and Organ Biodistribution Measurements. We next asked whether flycodes could also be used to simultaneously measure organ and tumor distribution for every antibody in a cassette-dosed animal. For a proof-of-concept experiment (Fig. 1), Lewis lung carcinoma (LLC) tumor, engineered to stably overexpress the human epidermal growth factor receptor (EGFR), were subcutaneously implanted into one flank of immunocompromised mice. On opposing flanks of the same mice, control LLC tumors not expressing EGFR were implanted. These mice were injected with a cassette of flycoded antibodies that included two EGFR binders: cetuximab, and an in-house generated sybody (synthetic nanobody) termed SB1382 (*SI Appendix*, Fig. S9 and Text S1). To prevent rapid elimination (22), SB1382 was fused to an albumin-binding DARPin (Dar-SB1382) (23) (*SI Appendix*, Text S1). To ensure inclusion at known concentrations, flycoded cetuximab and Dar-SB1382 were separately purified before being spiked-in to a bulk-purified flycoded pool containing 20 non-EGFR-binding antibodies. Flycoded cetuximab and Dar-SB1382 were added to the bulk antibody mix so as to be equivalent to the estimated average amount of antibody in the cassette. This flycoded antibody cassette was injected i.v. at a dose of 60 mg/kg into mice bearing LLC EGFR$^+$ on one flank and LLC EGFR$^-$ tumors on the other, ensuring maximal comparability of data within single animal. 24 h later mice were killed and LLC tumors were harvested, along with plasma, liver, kidney, spleen, and brain. Tissues were weighed and homogenized, followed by flycode extraction and LC–MS/MS analysis. Total flycode abundances were normalized to tissue or plasma masses and were used for determination of relative antibody or Dar-SB1382 accumulation. Comparison of mass-adjusted abundances in EGFR-positive and negative LLC tumors indicated that the EGFR binders cetuximab and Dar-SB1382 were significantly enriched in EGFR-positive tumor tissue, whereas all other flycoded antibodies were not (Fig. 3 *A* and *B*), indicating that flycodes allow simultaneous observation of multiple tumor-targeted protein drugs within a complex sample. For biodistribution analysis in organs, mass-adjusted tissue/plasma ratios were calculated (Fig. 3 *C* and *D* and *SI Appendix*, Fig. S10). A notable result was observed for liver homogenates, where a single antibody, volagidemab, was significantly enriched (Fig. 3 *C* and *D*). Intriguingly, volagidemab targets the human and mouse glucagon receptor (24, 25), a target that is abundantly expressed in the liver (26). Therefore, the observed nonlinear PK of volagidemab (Fig. 2*F*) can be explained by TMDD via glucagon receptor-mediated uptake. For all other organ homogenates, unambiguous specific accumulation was not observed for any antibody (*SI Appendix*,

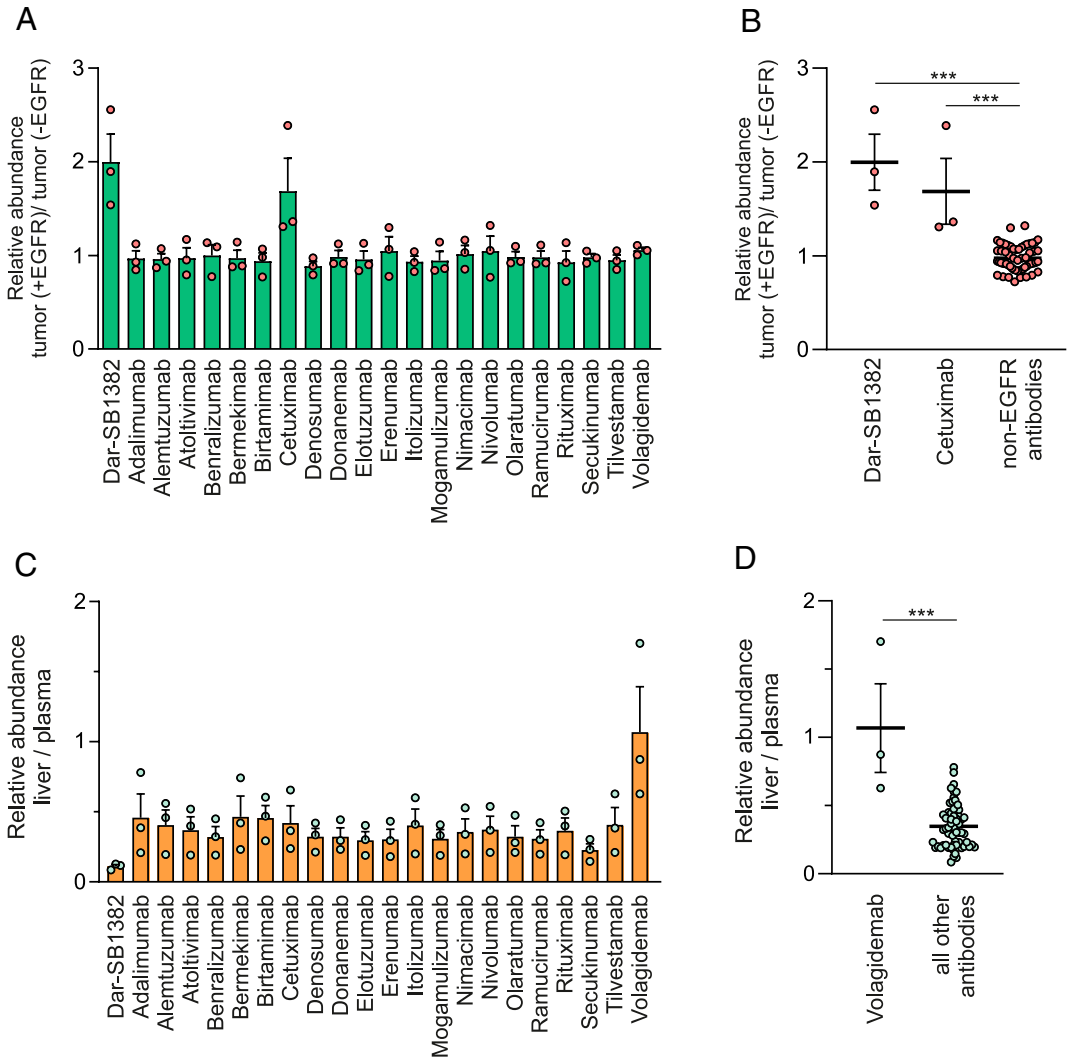

Fig. 3. Tumor and organ biodistribution. (*A* and *B*) Mice implanted with EGFR-expressing LLC tumors on one flank and EFGR-negative LLC tumors on the opposing flank were injected with a cassette of >20 flycoded antibodies. After 24 h, flycodes were extracted from excised tumors and quantitated with LC–MS/MS. Mass-adjusted antibody abundance ratios were determined (*A*) and indicated significant accumulation of EGFR binders Dar-SB1382 and cetuximab (*B*), ***$P < 0.001$ based on one-way ANOVA with Dunnett's multiple comparison test. (*C* and *D*) Flycode-derived tissue/plasma ratios were determined from liver homogenates (*C*), indicating specific accumulation of volagidemab (*D*), ***$P < 0.001$ based on two-tailed Student's *t* test. Data points are the average of three biological replicates, isolated from three different mice. Error bars are the SE of mean (s.e.m.).

Fig. S10). Flycode extraction from kidney homogenates showed generally elevated tissue/plasma ratios, as well as a high degree of variation between biological replicates, which could be related to differing levels of residual blood contamination within the particularly dense renal microvasculature network (27). In addition, the observation of exceptionally low tissue/plasma ratios for brain homogenates agrees with the low permeability of antibodies across the blood–brain barrier (28).

Characterization of a Pool of Drug-Like Bispecific DARPin-Sybody Molecules. In analogy to the early development phase of a biologic drug development pipeline, we isolated approximately 100 unique sybody clones from our in-house selection library (14, 29) and used them as proxies for drug candidates that are based on a single immunoglobulin scaffold thus are highly similar in polypeptide sequence. Plasmids encoding these sybodies were pooled and subcloned *en masse* into our C-terminal flycode library, and next-generation sequencing (NGS) was used to unambiguously assign flycode sets to associated sybodies (12). Next, all flycoded sybodies were genetically fused (N-terminally) to the aforementioned DARPin-based half-life extension module (23). The entire flycoded DARPin-sybody (Dar-SB) pool was expressed and purified from a single *Escherichia coli* culture and displayed biochemical characteristics befitting an individual standalone protein (*SI Appendix*, Fig. S11). For validation purposes, it included as well a spiked-in chemically biotinylated variant of one flycoded Dar-SB cassette member (Dar-SB355^{Biot}). To exhibit the versatility of flycodes for high-throughput biophysical characterization, a pool-based thermostability experiment was performed by exposing the Dar-SB pool to elevated temperatures ranging from 45 to 90 °C, followed by size exclusion chromatography (SEC) (Fig. 4*A*). As expected, the SEC peak became smaller in response to higher heat exposures due to aggregation of less robust pool members. Flycodes of the respective SEC peaks were isolated and analyzed by LC–MS/MS. For 80 Dar-SB pool members, at least 10 flycodes were detected by LC–MS/MS and thermal unfolding transition temperature (T_m) values were simultaneously determined for these reliably detected molecules (Fig. 4 *B* and *C*). Notably, the bulk T_m value for the entire pool, determined via integrated chromatographic peak areas ($T_m \approx 64$ °C), was similar to the

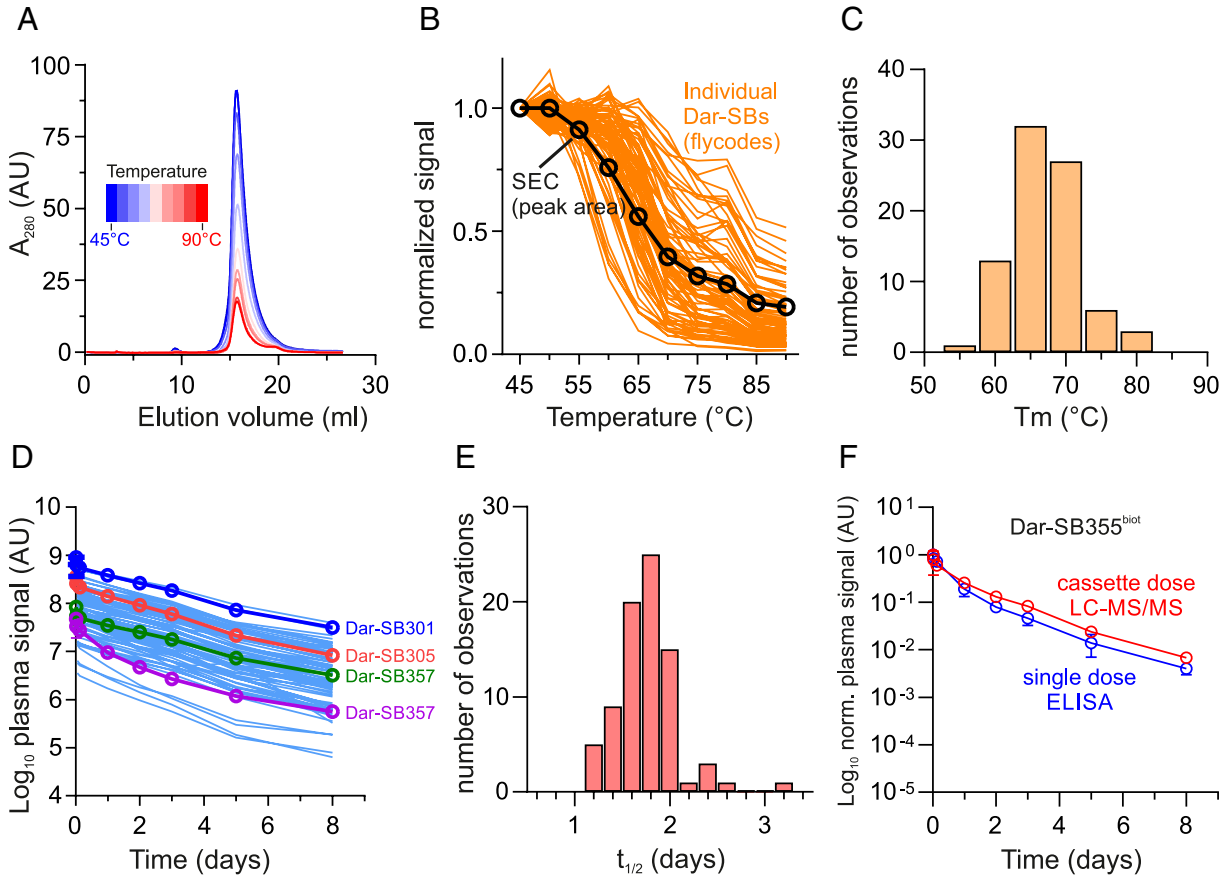

Fig. 4. Characterization of a large pool of drug-like DARPin-sybody constructs using flycodes. (*A–C*) Thermostability analysis. (*A*) SEC profiles for aliquots of the purified Dar-SB cassette (~100 flycoded constructs) that were heated at +5 °C increments from 45 to 90 °C. (*B*) Thermostability curves for the bulk Dar-SB pool, based on integrated SEC peak areas (black) and for individual members, based on LC–MS/MS determination of flycode abundances (orange). (*C*) Distribution of estimated Tm values. (*D–F*) Pharmacokinetic analysis. (*D*) Plasma decay curves for 80 Dar-SB constructs (thin blue lines) from cassette-dosed mice, with selected pool members highlighted (thick colored lines). Data points are averages from three biological replicates, and error bars representing SD were smaller than the data points. (*E*) Distribution of estimated half-life values. (*F*) Comparability of flycode detection from cassette dosing, with ELISA-based detection using single dosing. One member of the Dar-SB pool was produced as a single protein, purified, biotinylated, and spiked-into the cassette (Dar-SB355^{Biot}). In parallel, Dar-SB355^{Biot} was dosed as a single protein to control mice, and detected in plasma using ELISA. Data points represent average of three biological replicates (LC–MS/MS) or three technical replicates (ELISA), and error bars are SD.

average T_m value measured via LC–MS/MS flycode analysis for each Dar-SB construct ($T_m \approx 67$ °C, Fig. 4 *B* and *C*).

Cassette Dosing of ~100 Proteins in Mice and Determination of Individual Elimination Half-Lives. For pharmacokinetic analysis, the Dar-SB pool described above was administered intravenously to C57BL/6 mice at an overall dose of 54 mg/kg, corresponding to an estimated average per-construct dose of approximately 0.5 mg/kg, and plasma was sampled throughout an 8 d time course. Prior to flycode extraction from plasma, nine cassette-dosed mice were bundled into three groups, each containing three mice, and normalized plasma volumes from each group were combined for each timepoint. This cohort-bundle sample pooling was performed in order to ensure detection of a maximal number of Dar-SB constructs. Flycodes were extracted and quantitated with LC–MS/MS, and relative abundances were used to plot plasma abundance-time curves (Fig. 4*D*). As a conservative threshold, we only accepted Dar-SB constructs for which at least 10 flycodes were unambiguously identified, which resulted in a final tally of 80 Dar-SB entities which could be characterized with high confidence. For the remaining 20 Dar-SB, less than 10 flycodes were detected per construct either because the respective Dar-SB constructs were attached to a lower number of flycodes in the *en masse* cloning step, or because they were weakly expressed in the pool and consequently their flycodes were poorly detected by mass spectrometry (12). Calculated half-lives ranged from 1.2 to 3.1 d, with an average of 1.8 d (Fig. 4*E*), which is similar to reported values for mouse albumin (30, 31) as well as the DARPin module itself (23). These half-lives illustrate a ~100-fold increase relative to nonmodified nanobodies ($t_{1/2}$ = 0.01 to 0.04 d) (22) and demonstrate the effectiveness of the DARPin-based half-life extension strategy as well as the accuracy of flycode-based detection. In a final validation experiment, we observed that the normalized serum levels of single-dosed biotinylated Dar-SB355^{Biot} detected by ELISA are in close agreement to those measured from the cassette-dosing experiment detected by LC–MS/MS (Fig. 4*F*).

Discussion

Determination of PK/PD parameters is an enduring bottleneck of the biotherapeutic development pipeline, as it requires multiple animals in order to analyze each drug candidate. Moreover, in vivo drug behavior cannot be reliably predicted from in vitro properties. Theoretically, cassette dosing offers a solution to this problem, but limitations in detection throughput have constrained cassette sizes for protein therapeutics (9, 10). In this work, we have demonstrated a new strategy to overcome current restrictions of cassette dosing for efficient high-throughput PK and biodistribution analysis of antibodies and other protein biotherapeutics. Our proof-of-concept experiments have revealed that flycodes—specially

designed, genetically encoded peptide tags—allow full leveraging of the power of LC–MS/MS to accurately quantify thousands of peptides in a single complex mixture, which we exploited for the successful determination of PK parameters and biodistribution characteristics for dozens of drug-like proteins, from single cassette–dosed animals.

The main goal of our work was to show flycode-based PK/PD analysis involving cassette dosing of established antibody drugs, an application case which could help alleviate the combinatorial burden of assessing various possible antibody combination therapies, thereby addressing a topic of high clinical interest (32, 33). We applied flycode-based measurement to a pool of >20 marketed or advanced clinical-stage antibodies, representing molecules that possess excellent biophysical properties due to having been vetted by rigorous development pipelines. Our results demonstrated that PK parameters can be simultaneously determined for mixtures of monoclonal antibodies, giving parameter values that are in agreement with the PK characteristics of human IgGs. We also performed a tumor and organ biodistribution analysis, which showed specific accumulation for two EGFR-binding proteins (Cetuximab and Dar-SB1382) within EGFR-expressing tumors, in a single experiment. This target-dependent tumor accumulation, against the background of 20 other flycoded antibodies, provided solid evidence that flycodes do not interfere with biotherapeutic activity in vivo.

We noted large variabilities of PK parameters in a literature survey of human antibodies studied in mice, which is likely due to differences in experimental design (*SI Appendix*, Text S2 and Dataset S3). Presumably the greatest advantages of cassette-dosing is the simultaneous analysis of all members of the cassette pool in a single mouse under exactly the same experimental conditions, thereby allowing high-quality rank-ordering of PK or biodistribution properties. Such an approach can facilitate more efficient benchmarking of new biotherapeutic candidates against drugs with established PK and safety profiles.

Another aim of the present work was to address development constraints at the early stage of biotherapeutic drug discovery. Attempts have been made to empirically establish a basic set of favorable biophysical characteristics, known as developability profiles, which could be used to rank-order the typically large number of early-stage biotherapeutic candidates and thus rationally decide which candidates should be selected for further development (6, 7). AI and machine-learning approaches have also recently been successful in predicting antibodies that possess superior biophysical properties (34, 35). While such "de-risking" strategies are very useful for excluding candidates with exceedingly poor physicochemical properties, it has not yet been extended to in vivo characterization. Here, we demonstrated how flycode-based detection permits preclinical PK assessment of 80 drug-like half-life extended single-domain antibody constructs (Dar-SBs) from single cassette–dosed animals. We also demonstrated how flycodes can facilitate efficient in vitro biophysical screening, by the simultaneous one-pot determination of unfolding T_m values for all Dar-SB cassette pool members. However, other relevant biophysical properties such as self-association that influence viscosity, solubility, aggregation, and opalescence cannot be assessed in flycoded cassette pools, as they contain complex molecule mixtures. Importantly, due to the high similarity between constructs, reliance on endogenous tryptic peptides for LC–MS/MS detection would have been very challenging, in analogy to testing of a pool of antibodies of the same isotype generated against a single antigen. Overall, these experiments showed how flycodes can facilitate the preclinical screening of dramatically more biotherapeutic drug candidates than current practices allow, while reducing the ethical burdens of excessive animal usage and interexperimental variability (36). Remarkably, all cassette-dosing data shown in this study were obtained with only 18 mice, including replicates.

While experimental considerations regarding cassette dosing and LC–MS/MS have been described elsewhere (9, 37, 38), we wish to discuss here potential technical issues that may be caused by flycodes. Flycodes may alter biotherapeutic protein PK/PD in three potential ways: i) charge effects, ii) steric effects, or iii) effects owing to protein trafficking by signal sequence mimicking. Extra charges attributable to flycodes would result in estimated macroscopic isoelectric point (pI) shifts ranging from 0 to 0.3 pI units, depending on the specific flycode sequence (12). Since PK/PD is only measurably affected when introduced charge patches cause shifts of ≥ one pI unit (39), charge effects due to flycodes are not anticipated to have a significant impact. However, the His-tag that is part of our flycoded constructs could potentially modulate the pharmacodynamic behavior of macromolecules by binding to heparan sulfate present in the extracellular matrix and on cell surfaces (40). To assess the influence of the His-tag, other affinity tags may be tested in future studies. Steric effects of flycodes are also unlikely to be of concern, due to their small size (~25 residues, including protease cleavage sites and His-tag) relative to the attached biotherapeutic protein. The fact that antibody-drug conjugates often show comparable PK to the unmodified antibody (41), even at high drug:antibody coupling ratios (42), adds credence to the likely noninterference of flycodes, which have a precisely controlled 1:1 stoichiometry and C-terminal localization that is distal to functionally critical regions. While protein trafficking effects cannot be ruled out, we note that the multiplexed use of around 30 to 40 flycodes per biotherapeutic protein would likely mitigate any rare anomalous effects arising due to a particular flycode. Importantly, neither our data in this study, nor in our prior work (12), bears any indication of aberrations due to flycodes.

In conclusion, we have presented flycode-based LC–MS/MS detection as a powerful new method for protein biotherapeutic screening in laboratory animals. By using flycodes, high-throughput antibody screening can now be extended to the in vivo realm of preclinical PK and biodistribution analysis. Importantly, flycode-based experiments can be highly compatible with the ongoing rapid advancements in AI — since NGS data gives full sequence information for all flycoded biotherapeutics, large high-quality datasets can be generated from flycode experiments, which can be used for machine learning approaches in order to find potentially correlations between sequence-level in silico properties and observed PK/PD or biodistribution behavior. Overall, we anticipate that flycode-based analysis will help lowering the cost and timelines in preclinical development while increasing the success rate in bringing new protein biotherapeutics to market.

Materials and Methods

Production of Flycoded Monoclonal Antibody Expression Constructs. Publicly available protein sequences for 23 marketed or development-phase monoclonal antibodies (Dataset S1) were reverse-translated in silico with EMBOSS Backtranseq, (https://www.ebi.ac.uk/Tools/st/emboss_backtranseq/) using a *Homo sapiens* codon table, to produce DNA sequences which were chemically synthesized (GeneUniversal). Variants were also produced for two of the antibodies (denosumab and nivolumab) that encode the mutations H310A/H435Q (16) in the heavy chain constant region. All synthetic heavy and light-chain genes were flanked with SapI restriction sites to facilitate the use of FX cloning (12, 43). Additionally, the 5′ region of each synthetic ORF was preceded in-frame by a mammalian Kozak sequence (GCCACC) followed by an immunoglobulin secretion signal (translated signal sequences were the following:

MDWTWRVFCLLAVAPGAHS for heavy chains and MVLQTQVFISLLLWISGAYG for light chains). Each heavy chain ORF was subcloned, in one-pot reactions, into a discrete set of 30 to 50 unique FX-compatible pNLx flycode destination vectors (12), resulting in each heavy chain being variably fused to 30 to 50 possible independent flycodes (see section "Production of predetermined flycode sets for individual antibody tagging"). Dataset S1 indicates the correspondences between antibodies and flycode set identifiers (which link to flycode sequences in FASTA database p3678_db1). Ultimately, the C-terminus of all heavy chains consisted of: [thrombin cleavage site]-[flycode]-[trypsin cleavage site]-[10xHis], whereas light chains were unmodified. All constructs were subcloned into pcDNA3.4-derived expression vectors under the control of the CMV promoter, and transfection-grade plasmid DNA was prepared using a NucleoBond Xtra midiprep kit (Macherey-Nagel).

Expression and Purification of Flycoded Antibodies. Flycoded antibodies were expressed individually using suspension Expi293 cells (ThermoFisher). Transfections were carried out using the Expifectamine 293 transfection kit (ThermoFisher), following the manufacturer protocol, using a 1:1 mass ratio of heavy:light chain plasmid DNA. Expression was allowed to proceed for 6 d at 37 °C in a humidified shaker maintained at 8% CO_2. The flycoded antibodies were purified from culture supernatant via their His-Tag using NiNTA chromatography, followed by SEC (SRT SEC-300, Sepax). Endotoxin was depleted using the Triton X-114 phase separation technique (44). FC-cetuximab, FC-alemtuzumab, and FC-rituximab (and the corresponding nonflycoded counterparts alemtuzumab and rituximab) for single-dosed mice experiments were prepared similarly (for details, see *SI Appendix*, Text S3). Clinical grade nonflycoded Cetuximab (Erbitux®, Merck (Schweiz) AG) was a generous gift by H. Läubli, University Hospital Basel, Switzerland. Further details about the purification of flycoded antibodies are provided in *SI Appendix*, Text S3.

Discovery and Characterization of EGFR-Binding Sybody SB1382. The SB1382 sybody targeting the EGFR was produced from an in vitro selection campaign against detergent-solubilized human EGFR (45), using a previously described sybody selection protocol (29). SB1382 was expressed in *E. coli* MC1061 cells using the vector pSBinit (Addgene #110100) and purified using NiNTA affinity chromatography (Qiagen) and SEC (SRT SEC-100, Sepax) (29). Note that this expression construct adds a Myc-tag C-terminal to the sybody sequence.

Flow Cytometry Characterization of EGFR Binding. To verify EGFR binding we have used human endogenously EGFR-expressing A431 cell line as target cells (46). Cells were grown in DMEM (Sigma) supplemented with 10% heat-inactivated fetal calf serum (Pansera), 1% L-glutamine (Thermo Fisher Scientific), and 1% Penicillin-Streptomycin (PAA Laboratories). To determine the binding, cells were scraped from the vessel surface and incubated in PBS in presence of 5 μg/mL of Myc-tagged sybodies for 20 min, then washed and incubated for 20 min with anti-c-Myc-tag antibody (Thermo Fisher Scientific) in presence of live/dead staining (Biolegend). As positive control, a fluorescently labeled anti-EGFR antibody was used (Biolegend). Samples were acquired using LSRII Fortessa (Becton, Dickinson and Company) and analyzed using FlowJo Software v10 (Becton, Dickinson and Company).

Flycoding of SB1382, DARPin Fusion, and Expression/Purification. Flycodes were appended to the C-terminus of SB1382 using an equivalent one-pot strategy as described above for the construction of flycoded antibodies (flycodes associated with SB1382 are identified via header P1B1 in FASTA database p1875_db11). Flycoded SB1382 was then excised from pNLx via flanking SfiI sites and ligated into a custom expression vector (pDar1) harboring a coding sequence for a previously described albumin-binding DARPin (23) (Dar), preceded by the signal sequence of *E. coli* DsbA for periplasmic secretion (47), and followed by the linker $(GGGGS)_3$GGA. Importantly, after bacterial transformation of the ligation mixture and plating on LB-agar containing 50 μg/mL kanamycin, approximately 500 cfu were scraped from the plate for liquid culture inoculation and plasmid preparation; this high number of colonies ensures that all flycodes will be retained. The resulting ORF, designated as Dar-SB1382, encoded a fusion protein consisting of Dar-$(GGGGS)_3$GGA-SB1382-[thrombin cleavage site]-[variable flycode]-[trypsin cleavage site]-[10xHis]. For expression, transformed *E. coli* MC1061 cells were grown at 37 °C in 3 × 600 mL Terrific Broth supplemented with 50 μg/mL kanamycin and expression was induced via addition of 0.05% (w/v) arabinose at OD_{600} = 0.6. After overnight expression at 18 °C, cells were harvested, resuspended with 100 mL TBS (20 mM Tris-HCl, pH 7.5, 150 mM NaCl) and lysed with a microfluidizer high-shear homogenizer (Microfluidics). After removal of debris via centrifugation, the soluble lysate was supplemented with 15 mM imidazole and stirred with 5 mL of NiNTA affinity resin (Qiagen) for 1 h. The resin was transferred to a gravity column and washed with 150 TBS + 15 mM imidazole, followed by elution with 300 mM imidazole and injection onto an SRT SEC-300 size exclusion column (Sepax) equilibrated in PBS, where Dar-SB1382 eluted as a single peak. Endotoxin was depleted using the Triton X-114 phase separation technique (44) and Dar-SB1382 was stored at 4 °C.

Production of Predetermined Flycode Sets for Individual Antibody Tagging. DB3.1 cells were transformed with an aliquot of the pNLx flycode library (total diversity ~ 10^8) (12) and 3,072 individual clones were picked and used to inoculate individual 1.0 mL LB-chloramphenicol cultures in 32 96-well deep-well plates, and were grown with shaking at 37 °C overnight. The next day, 30 uL of 32 individual unique cultures were combined in each well of a fresh 96-well deep-well plate, theoretically resulting in each well containing 32 bacterial clones harboring unique pNLx flycode vectors. A plasmid miniprep was prepared for each well, and these plasmids were transferred to a new 96-well plate (hereafter termed "flycode plate"). Next, genes encoding 24 unique sybodies of known sequence (from an in-house collection) were subcloned into 24 separate pNLx plasmid sets from the flycode plate. These 24 unique sybody-flycode sets were pooled into a single tube and subjected to NGS as described previously (12). This process was repeated three times, resulting in four separate NGS pools and complete coverage of the flycode plate. The unique known identity of each sybody subsequently allowed for assignment of flycodes within each analyzed 24-well index of the flycode plate.

Bulk Isolation, Flycoding, and DARPin Fusion Generation of Approximately 100 Sybodies. To generate a pool of single-domain antibodies for mimicry of the discovery phase of a drug development pipeline, approximately 100 cfu of single sybody clones from a typical selection campaign (14) were isolated and pooled. These 100 cfu were inoculated into a single LB-chloramphenicol culture and plasmid was isolated using a NucleoBond Xtra midiprep kit (Macherey-Nagel). This pool of sybody genes was "nested" into a pool of pNLx flycode vectors in a single reaction, as previously described (12), in order to tag every sybody in average with 30 flycodes. A previously described NGS approach using Illumina Mi-Seq was followed to assign the flycodes to the respective sybody clone of the nested pool (12). Fusion of the albumin-binding DARPin (Dar) was achieved using the same procedure as described above for SB1382. In short, the pooled, flycoded sybody genes were excised from pNLx via SfiI digestion, and this fragment pool was ligated into the pDar1 vector followed by bacterial transformation.

Dar-SB Cassette Pool Production for Mouse PK Experiments. Expression and purification of the Dar-SB pool was also performed as described above for Dar-SB1382, entailing expression from a single *E. coli* MC1061 culture, followed by NiNTA affinity chromatography and SEC. As a control construct, one pool member, Dar-SB355, was independently flycoded (FASTA identifier P1G3), expressed and purified. This standalone flycoded Dar-SB355 construct was then chemically biotinylated using EZ-Link™ NHS-Biotin (Thermo Fisher Scientific). Biotinylated Dar-SB355 (Dar-SB355Biot) was then spiked-in to the purified, flycoded Dar-SB pool. Finally, this Dar-SB cassette pool was subjected to endotoxin depletion and filtering, and was then directly used for mouse injections.

Thermostability Assay. The purified Dar-SB pool (1.2 mg/mL, in average 0.01 mg/mL per construct) was divided into ten 0.5 mL aliquots. Each aliquot was heated at a specific temperature (45 to 90 °C, in 5 °C increments) for 10 min, followed by centrifugation at 17,000×*g* to pellet any aggregated material. The soluble supernatant was then injected onto a SEC SRT-300 size exclusion column (Sepax) equilibrated in PBS. Integrated chromatogram peaks were used to calculate a bulk thermal denaturation curve for the entire Dar-SB pool. Subsequently, peak fractions corresponding to each temperature were pooled, concentrated to 380 μL, and 50 μL of each sample was subjected to flycode extraction (see below) and LC–MS/MS analysis (see below). Summed flycode intensities corresponding to each pool member were used to calculate individual thermal denaturation curves for all Dar-SB constructs.

Animals. Mice (C57BL/6 J) were obtained from Janvier Labs (Le Genest-Saint-Isle, France). All procedures described in the present study have been approved by the Cantonal Veterinarian's Office of Zurich (License ZH200/2017), and all efforts were made to minimize the number of animals used and to ensure animal welfare. Animals were killed by controlled CO_2 asphyxiation.

Plasma Isolation. For plasma isolation, blood was collected from tail vein in tubes containing sodium citrate 3.8% w/v, pH=8.4, spun down 5 min, 10,000×*g*, and plasma was transferred and frozen in 96-well microplates (Abgene) at −20 °C.

Mouse Pharmacokinetic Experiments. 6- to 10-wk-old mice were injected intravenously into the tail vein with binder pool prepared in PBS to reach doses of either 60 mg/kg or 15 mg/kg, assuming the average mouse weight being 20 g. Plasma samples were collected and used for flycode extraction. Flycodes were quantitated using LC–MS/MS (described below) and antibody abundances were derived from summed flycode intensities. For antibody PK, internal antibody-flycode standards were used to construct a calibration curve and convert LC–MS/MS-derived abundance values into antibody plasma concentrations. PKSolver (17) was used to estimate elimination half-life ($t_{1/2}$), area under the curve (AUC), clearance (C_L), mean residence time, and volume of distribution at steady state (V_{ss}). For Dar-SB PK, no internal calibration standards were used and normalized abundance values were directly used for estimation of $t_{1/2}$ using PKSolver. Outliers were removed from the final analysis based on the Grubbs' test on exposure (area under the curve) and $t_{1/2}$ data (GraphPad Prism version 10.4.0 for macOS, GraphPad Software, Boston, MA).

Generation of LLC EGFR (+) Cell Line. Pools of unselected LLC EGFR(+) and LLC EGFR(−) control cells were generated by transduction of parental LLC cells with constructs containing red fluorescent protein (RFP) and human EGFR with deleted intracellular signaling domain. Cells were cultured in DMEM (Sigma) with 10 % heat-inactivated fetal calf serum (Pansera), 1 % L-glutamine (Thermo Fisher Scientific) and 1 % Penicillin-Streptomycin (PAA Laboratories), and monoclonal lines were established by serial dilution under selective pressure from 200 μg/mL geneticin (Thermo Fischer Scientific). Clones with highest EGFR signal were selected by flow cytometry. The LLC EGFR(+) and LLC EGFR(−) monoclonal cell lines were selected to have matching RFP expression levels.

Tumor Implantation. For tumor cell implantation, 6- to 10-wk-old mice were anesthetized using isoflurane, back skin was shaved and LLC EGFR(−) tumor cells were injected subcutaneously into one flank, whereas LLC EGFR(+) cells into the opposite flank. Each tumor injection was performed at 200,000 cells/mouse, in PBS.

Mouse Biodistribution Experiments. Tumor bearing mice with each tumor [LLC EGFR(-) and LLC EGFR(+)] reaching size >55 mm^2 were injected intravenously into the tail vein with binder pool prepared in PBS to reach a dose of 60 mg/kg. After 24 h, mice were killed, plasma was collected, and the liver, kidney, spleen brain, and both tumors were dissected and frozen at −20 °C.

Sample Preparation for Flycode Extraction. For antibody PK, collected plasma samples (5 to 30 μL) were diluted into 1.0 mL of buffer EX (20 mM Tris-HCl, pH 7.4, 150 mM NaCl, 10 mM imidazole, 0.25% Triton X-100). For absolute quantification, a separately purified, flycoded antibody was added (for details, see *SI Appendix*, Text S3).

For antibody biodistribution, collected tissue samples from tumor mice killed 24 h postinjection were homogenized in a glass vial using a teflon pestle and subsequently solubilized using Triton X-100.

Debris was removed and supernatants were passed through 0.45 μm centrifugal filters (Millipore). For further details, see *SI Appendix*, Text S3.

All Dar-SB samples were extracted in buffers containing 0.25% Triton X-100 and 4.5 M guanidinium chloride. For further details, see *SI Appendix*, Text S3.

Flycode Extraction. Flycode extraction was performed using modifications of a previously described protocol (12). In brief, flycoded antibodies or Dar-SB were captured using NiNTA-resin, followed by thrombin cleavage to separate flycode from antibody or Dar-SB, respectively. Flycodes with the His-tag still attached were eluted from the NiNTA-resin and passed through filters having a 10 kDa cutoff, followed by trypsin digestion to separated flycode from His-tag. For further details, see *SI Appendix*, Text S3.

Sample Preparation for Comparison of Endogenous Tryptic Peptides and Flycodes. For the experiments comparing detection based on endogenous tryptic peptides with flycode-based detection (*SI Appendix*, Fig. S2), we used the same purified antibody cassette as was used for biodistribution studies (*SI Appendix*, Text S3). In separate reactions, either 12 μg or 4 μg of flycoded antibody pool (stock concentration 6.7 mg/mL) was diluted into 250 μL of buffer TRY (20 mM triethylammonium bicarbonate (TEAB), pH 8.5, 150 mM NaCl, 2.5 mM $CaCl_2$). 1 μg of trypsin (Promega) was added and samples were incubated overnight at 37 °C. Note that trypsin cleaves the thrombin cleavage site exactly where thrombin does, namely after the arginine (LVPR/GS). No flycode enrichment or filtering was performed for this control experiment, and these samples were used directly for StageTip preparation preceding LC–MS/MS analysis.

LC–MS/MS Analysis. For LC–MS/MS analysis, the flycode peptides were further purified by StageTip containing a reverse-phase matrix (3 M™ C18 Extraction Disks), supplemented with indexed retention time (iRT) standard peptides (2xiRT kit, Biognosys), separated on a reversed-phase analytical column (nanoEase M/Z HSS T3) and measured on Orbitrap Fusion or Orbitrap Fusion Lumos mass spectrometers (Thermo Fisher Scientific), operated in positive ionization and direct data acquisition modes. Further details are provided in *SI Appendix*, Text S3.

LC–MS/MS Data Processing. LC–MS/MS data were analyzed using programs Progenesis QI (Nonlinear Dynamics), Mascot 2.5 (Matrix Science), and Scaffold. The detailed procedure is provided in *SI Appendix*, Text S3.

ELISA Measurements. For the ELISA measurements of flycoded and nonflycoded alemtuzumab, rituximab, and cetuximab in plasma from single-dose control mice, antibody-specific affinity reagents (obtained from Bio-Rad) were used in a sandwich-ELISA set-up as further specified in *SI Appendix*, Text S3.

To detect Dar-$SB355^{Biot}$ in plasma from single-dose control mice, the bispecific DARPin-sybody molecule was captured via neutravidin on an ELISA plate and detected via an anti-polyHistidine-peroxidase antibody (details provided in *SI Appendix*, Text S3).

Data, Materials, and Software Availability. Mass spectrometry data as well as NGS-derived sequence databases are available from ProteomeXchange via the PRIDE partner repository under the identifiers PXD036658 (flycodes vs. endogenous tryptic peptides) (48), PDX036734 (antibody pharmacokinetics, cassette dose A) (49), PXD036661 (antibody pharmacokinetics, cassette dose B) (50), PXD036662 (tumor/organ biodistribution) (51), PXD036666 (Dar-SB thermostability) (52), and PXD036668 (Dar-SB pharmacokinetics) (53). All other data are included in the manuscript and/or supporting information.

ACKNOWLEDGMENTS. We thank Bernd Roschitzki, Laura Kunz, and Jonas Grossmann from the Functional Genomics Center Zurich for extensive assistance regarding LC–MS/MS data acquisition and processing. We thank Roger Dawson for providing scientific suggestions, Sujani Thavarasah for preparing Fig. 1 and Thorsten Buch for discussions at the early stages of the project. This project was supported by a SNSF BRIDGE proof of concept grant (20B1-1_175192, to P.E.) and a BioEntrepreneur-Fellowship of the University of Zurich (BIOEF-17-002, to I.Z.), the European Research Council (ERC) (consolidator grant no. 772190, to M.A.S.), and an SNSF Professorship of the Swiss NSF (PP00P3_144823, to M.A.S.). J.v.B. is supported through grants of the Novartis Foundation for Medical-Biological Research (16C231), Swiss Life Jubiläumsstiftung (1283-2021), Swiss NSF (NRP79, 407940_206465), Lindonlight Collective LLC (GR-24-010) and Swiss Cancer Research (KFS-3852-02-2016, KFS-4146-02-2017, KFS-5306-02-2021). S.K. received funding from the European Research Council (ERC) (CoG 101124203). S.K. is supported by "i-Target: immunotargeting of cancer" (funded by the Elite Network of Bavaria), Melanoma Research Alliance (grant number 409510 to S.K.), Marie Sklodowska-Curie Training Network for Optimizing Adoptive T Cell Therapy of Cancer (funded by the Horizon 2020 programme of the European Union; grant 955575), Else Kröner-Fresenius-Stiftung, German Cancer Aid, the Wilhelm-Sander-Stiftung, Ernst Jung Stiftung, Institutional Strategy LMU excellent of Ludwig Maximilian University of Munich (within the framework of the German Excellence Initiative), the Go-Bio-Initiative, the m4-Award of the Bavarian Ministry for Economical Affairs, Bundesministerium für Bildung und Forschung, ERC (Starting Grant 756017 and PoC Grant 101100460), Deutsche Forschungsgemeinschaft (DFG; KO5055-2-1 and 510821390), by the SFB-TRR 338/1 2021–452881907, Fritz-Bender Foundation, Deutsche José Carreras Leukämie Stiftung and Hector Foundation.

Author affiliations: [a]Institute of Medical Microbiology, University of Zurich, Zurich 8006, Switzerland; [b]Institute of Laboratory Animal Science, University of Zurich, Schlieren 8952, Switzerland; [c]Linkster Therapeutics AG, Zurich 8006, Switzerland; [d]Division of Clinical Pharmacology, University Hospital, Ludwig Maximilian University of Munich, Munich 80337, Germany; [e]Einheit für Klinische Pharmakologie, Research Center for Environmental Health, Neuherberg 85764, Germany; and [f]German Cancer Consortium, Partner Site Munich, Munich 80337, Germany

Author contributions: J.D.W., M.B., P.E., I.Z., J.v.B., and M.A.S. designed research; J.D.W., M.B., P.E., I.Z., L.M.H., and F.A. performed research; M.S. and S.K. contributed new reagents/analytic tools; J.D.W., M.B., P.E., I.Z., L.M.H., F.A., J.v.B., and M.A.S. analyzed data; and J.D.W., M.B., J.v.B., and M.A.S. wrote the paper.

Competing interest statement: P.E., I.Z. and M.A.S. are founders and shareholders of Linkster Therapeutics AG. P.E., I.Z. and M.A.S. are inventors of patent WO2018078167A1. M.B. and J.v.B. are named inventors on patents in the field of immuno-oncology. M.B. and J.v.B. are part time employees and have equity interest in InCephalo AG. J.v.B. has received honoraria from Bristol Myer Squibb. S. K. has received honoraria from TCR2 Inc., Cymab, Plectonic, Miltenyi, Galapagos, Novartis, BMS and GSK. S. K. is an inventor of several patents in the field of immuno-oncology. S. K. received license fees from TCR2 Inc and Carina Biotech. S.K. received research support from TCR2 Inc., Tabby Therapeutics, Catalym GmBH, Plectonic GmBH and Arcus Bioscience for work unrelated to the manuscript.

1. R.-M. Lu *et al.*, Development of therapeutic antibodies for the treatment of diseases. *J. Biomed. Sci.* **27**, 1–30 (2020).
2. P. J. Carter, G. A. Lazar, Next generation antibody drugs: Pursuit of the'high-hanging fruit'. *Nat. Rev. Drug Discov.* **17**, 197–223 (2018).
3. K. Škrlec, B. Štrukelj, A. Berlec, Non-immunoglobulin scaffolds: A focus on their targets. *Trends Biotechnol.* **33**, 408–418 (2015).
4. A. F. Labrijn, M. L. Janmaat, J. M. Reichert, P. W. Parren, Bispecific antibodies: A mechanistic review of the pipeline. *Nat. Rev. Drug Discov.* **18**, 585–608 (2019).
5. S. Yamaguchi, M. Kaneko, M. Narukawa, Approval success rates of drug candidates based on target, action, modality, application, and their combinations. *Clin. Transl. Sci.* **14**, 1113–1122 (2021).
6. M. Bailly *et al.*, Predicting antibody developability profiles through early stage discovery screening. *MAbs* **12**, 1743053 (2020).
7. T. Jain *et al.*, Biophysical properties of the clinical-stage antibody landscape. *Proc. Natl. Acad. Sci. U.S.A.* **114**, 944–949 (2017).
8. L. W. Frick, K. K. Adkison, K. J. Wells-Knecht, P. Woollard, D. M. Higton, Cassette dosing: Rapid in vivo assessment of pharmacokinetics. *Pharm. Sci. Technol. Today* **1**, 12–18 (1998).
9. H. Li *et al.*, Simultaneous analysis of multiple monoclonal antibody biotherapeutics by LC-MS/MS method in rat plasma following cassette-dosing. *AAPS J.* **15**, 337–346 (2013).
10. M. Nagayasu, K. Ozeki, Combination of cassette-dosing and microsampling for reduced animal usage for antibody pharmacokinetics in cynomolgus monkeys, wild-type mice, and human FcRn transgenic mice. *Pharm. Res.* **38**, 583–592 (2021).
11. J. C. Stüber *et al.*, Impact of charge patches on tumor disposition and biodistribution of therapeutic antibodies. *AAPS Open* **8**, 1–18 (2022).
12. P. Egloff *et al.*, Engineered peptide barcodes for in-depth analyses of binding protein libraries. *Nat. Methods* **16**, 421–428 (2019).
13. H. K. Binz, M. T. Stumpp, P. Forrer, P. Amstutz, A. Plückthun, Designing repeat proteins: Well-expressed, soluble and stable proteins from combinatorial libraries of consensus ankyrin repeat proteins. *J. Mol. Biol.* **332**, 489–503 (2003).
14. I. Zimmermann *et al.*, Synthetic single domain antibodies for the conformational trapping of membrane proteins. *eLife* **7**, e34317 (2018).
15. R. J. Boado, Y. Zhang, Y. Wang, W. M. Pardridge, Engineering and expression of a chimeric transferrin receptor monoclonal antibody for blood–brain barrier delivery in the mouse. *Biotechnol. Bioeng.* **102**, 1251–1258 (2009).
16. V. Kenanova *et al.*, Tailoring the pharmacokinetics and positron emission tomography imaging properties of anti–carcinoembryonic antigen single-chain Fv-Fc antibody fragments. *Cancer Res.* **65**, 622–631 (2005).
17. Y. Zhang, M. Huo, J. Zhou, S. Xie, PKSolver: An add-in program for pharmacokinetic and pharmacodynamic data analysis in Microsoft Excel. *Comput. Methods Programs Biomed.* **99**, 306–314 (2010).
18. W. Wang, E. Wang, J. Balthasar, Monoclonal antibody pharmacokinetics and pharmacodynamics. *Clin. Pharmacol. Ther.* **84**, 548–558 (2008).
19. J. A. Reijers, M. J. Dane, A. J. van Zonneveld, J. Burggraaf, M. Moerland, Potential influence of endothelial adsorption on the delayed time to maximum concentration of biopharmaceuticals. *Eur. J. Drug Metab. Pharmacokinet.* **43**, 103–113 (2018).
20. J. A. Reijers, M. Moerland, J. Burggraaf, Remarkable pharmacokinetics of monoclonal antibodies: A quest for an explanation. *Clin. Pharmacokinet.* **56**, 1081–1089 (2017).
21. A. V. Kamath, Translational pharmacokinetics and pharmacodynamics of monoclonal antibodies. *Drug Discov. Today: Technol.* **21**, 75–83 (2016).
22. S. Hoefman, I. Ottevaere, J. Baumeister, M. L. Sargentini-Maier, Pre-clinical intravenous serum pharmacokinetics of albumin binding and non-half-life extended Nanobodies®. *Antibodies* **4**, 141–156 (2015).
23. D. Steiner *et al.*, Half-life extension using serum albumin-binding DARPin® domains. *Protein Eng. Des. Sel.* **30**, 583–591 (2017).
24. J. Pettus *et al.*, Effect of a glucagon receptor antibody (REMD-477) in type 1 diabetes: A randomized controlled trial. *Diabetes, Obesity Metab.* **20**, 1302–1305 (2018).
25. M.-Y. Wang *et al.*, Glucagon receptor antibody completely suppresses type 1 diabetes phenotype without insulin by disrupting a novel diabetogenic pathway. *Proc. Natl. Acad. Sci. U.S.A.* **112**, 2503–2508 (2015).
26. C. Longuet *et al.*, Liver-specific disruption of the murine glucagon receptor produces α-cell hyperplasia: Evidence for a circulating α-cell growth factor. *Diabetes* **62**, 1196–1205 (2013).
27. H. Rafidi *et al.*, Effect of molecular size on interstitial pharmacokinetics and tissue catabolism of antibodies. *Mabs* **14**, 2085535 (2022).
28. L. A. Lampson, Monoclonal antibodies in neuro-oncology: Getting past the blood-brain barrier. *MAbs* **3**, 153–160 (2011).
29. I. Zimmermann *et al.*, Generation of synthetic nanobodies against delicate proteins. *Nat. Protocols* **15**, 1707–1741 (2020).
30. C. Chaudhury *et al.*, The major histocompatibility complex–related Fc receptor for IgG (FcRn) binds albumin and prolongs its lifespan. *J. Exp. Med.* **197**, 315–322 (2003).
31. B. Yang, J. C. Kim, J. Seong, G. Tae, I. Kwon, Comparative studies of the serum half-life extension of a protein via site-specific conjugation to a species-matched or-mismatched albumin. *Biomater. Sci.* **6**, 2092–2100 (2018).
32. T. A. Mace *et al.*, IL-6 and PD-L1 antibody blockade combination therapy reduces tumour progression in murine models of pancreatic cancer. *Gut* **67**, 320–332 (2018).
33. A. Baum *et al.*, Antibody cocktail to SARS-CoV-2 spike protein prevents rapid mutational escape seen with individual antibodies. *Science* **369**, 1014–1018 (2020).
34. S. Bachas *et al.*, Antibody optimization enabled by artificial intelligence predictions of binding affinity and naturalness. bioRxiv [Preprint] (2022) (Accessed 30 June 2023).
35. D. M. Mason *et al.*, Optimization of therapeutic antibodies by predicting antigen specificity from antibody sequence via deep learning. *Nat. Biomed. Eng.* **5**, 600–612 (2021).
36. B. Baertschi, M. Gyger, Ethical considerations in mouse experiments. *Curr. Protocols Mouse Biol.* **1**, 155–167 (2011).
37. W. Fu, B. An, X. Wang, J. Qu, Key considerations for LC–MS analysis of protein biotherapeutics in tissues. *Bioanalysis* **9**, 1349–1352 (2017)
38. R. Jenkins *et al.*, Recommendations for validation of LC-MS/MS bioanalytical methods for protein biotherapeutics. *AAPS J.* **17**, 1–16 (2015).
39. C. A. Boswell *et al.*, Effects of charge on antibody tissue distribution and pharmacokinetics. *Bioconjugate Chem.* **21**, 2153–2163 (2010).
40. H. M. Lacy, R. D. Sanderson, 6xHis promotes binding of a recombinant protein to heparan sulfate. *BioTechniques* **32**, 254–258 (2002).
41. C. Zhou *et al.*, Pharmacokinetics and pharmacodynamics of DSTA4637A: A novel THIOMAB™ antibody antibiotic conjugate against *Staphylococcus aureus* in mice. *MAbs* **8**, 1612–1619 (2016).
42. K. J. Hamblett *et al.*, Effects of drug loading on the antitumor activity of a monoclonal antibody drug conjugate. *Clin. Cancer Res.* **10**, 7063–7070 (2004).
43. E. R. Geertsma, R. Dutzler, A versatile and efficient high-throughput cloning tool for structural biology. *Biochemistry* **50**, 3272–3278 (2011).
44. Y. Aida, M. J. Pabst, Removal of endotoxin from protein solutions by phase separation using Triton X-114. *J. Immunol. Methods* **132**, 191–195 (1990).
45. C. J. Wikstrand *et al.*, Monoclonal antibodies against EGFRvIII are tumor specific and react with breast and lung carcinomas and malignant gliomas. *Cancer Res.* **55**, 3140–3148 (1995).
46. F. N. Zhang *et al.*, Quantification of epidermal growth factor receptor expression level and binding kinetics on cell surfaces by surface plasmon resonance imaging. *Anal. Chem.* **87**, 9960–9965 (2015).
47. D. Steiner, P. Forrer, M. T. Stumpp, A. Pluckthun, Signal sequences directing cotranslational translocation expand the range of proteins amenable to phage display. *Nat. Biotechnol.* **24**, 823–831 (2006).
48. J. Walter *et al.*, Proteomics data used for generation of SI Appendix, Fig. S4; Comparison of flycodes vs. unique endogenous tryptic peptides for antibody identification. The PRoteomics IDEntifications (PRIDE) database. https://www.ebi.ac.uk/pride/archive/projects/PXD036658. Deposited 12 September 2022.
49. J. Walter *et al.*, Proteomics data used for generation of Dataset S2; Antibody PK, cassette dose A (high dose). The PRoteomics IDEntifications (PRIDE) database. https://www.ebi.ac.uk/pride/archive/projects/PXD036734. Deposited 14 September 2022.
50. J. Walter *et al.*, Proteomics data used for generation of Dataset S2; Antibody PK, cassette dose B (low dose). The PRoteomics IDEntifications (PRIDE) database. https://www.ebi.ac.uk/pride/archive/projects/PXD036661. Deposited 12 September 2022.
51. J. Walter *et al.*, Proteomics data used for generation of Fig. 3 and SI Appendix, Fig. S10; Antibody tumor/organ biodistribution. The PRoteomics IDEntifications (PRIDE) database. https://www.ebi.ac.uk/pride/archive/projects/PXD036662. Deposited 12 September 2022.
52. J. Walter *et al.*, Proteomics data used for generation of Fig. 4 B and C; Dar-SB thermostability. The PRoteomics IDEntifications (PRIDE) database. https://www.ebi.ac.uk/pride/archive/projects/PXD036666. Deposited 12 September 2022.
53. J. Walter *et al.*, Proteomics data used for generation of Fig. 4 D and E; Dar-SB PK. The PRoteomics IDEntifications (PRIDE) database. https://www.ebi.ac.uk/pride/archive/projects/PXD036668. Deposited 12 September 2022.